RESEARCH

Mechanical behavior of coal under true triaxial loading test connecting the effect of excavation- and mining-induced disturbances

Mingzhong Gao · Xuemin Zhou · Xuan Wang · Jing Xie · Chen Wang · Qi Zhang · Heqiang Lv · Chenchen Guo

Abstract In order to understand the mechanical behavior of a stope and analyse the stress conditions of surrounding rocks after ventilation shaft excavation and the abutment stresses of the top coal mining layout. In situ uniaxial stress monitoring tests were performed to understand the field abutment pressure evolution. Furthermore, the variation of the stress concentration factor was studied using the Tongxin Mine 8309 mining face of the TongMei Group, China, as a case study. A loading model of coal rock under excavation- and mining-induced disturbances was proposed, and the stress path and experimental method were designed to investigate the high excavation-damaged zone (HDZ), excavation-damaged zone (EDZ), and undisturbed zone (UZ). Moreover, the mechanical characteristics and failure characteristics of coal rock in different zones under site disturbance were obtained and the mesoscopic analysis is carried out by acoustic emission test. The results indicated that the strengths of the UZ, EDZ, and HDZ samples declined gradually. The volume of the UZ sample continuously expanded. However, the volumes of the EDZ and HDZ samples were compressed first and then expanded. Furthermore, the shear bands presented in all three samples resulted in failure. The cubic triaxial tests performed without considering mining-induced pressure produced higher strengths and less damage compared with the results of the true triaxial tests. The stress path used in the laboratory with the mining-induced stress throughout the stope could optimally reproduce the in situ mining process, which is significantly safe and efficient for the mining of deep resources.

M. Gao · X. Zhou (✉) · X. Wang
Guangdong Provincial Key Laboratory of Deep
Earth Sciences and Geothermal Energy Exploitation
and Utilization, Institute of Deep Earth Sciences
and Green Energy, College of Civil and Transportation
Engineering, Shenzhen University, Shenzhen 518060,
China
e-mail: zhouxuemin2021@email.szu.edu.cn

M. Gao · J. Xie
State Key Laboratory of Hydraulics and Mountain River
Engineering, College of Water Resource and Hydropower,
Sichuan University, Chengdu 610065, China

C. Wang · Q. Zhang · H. Lv · C. Guo
State Key Laboratory of Coal Mining and Clean
Utilization, Beijing 100013, China

Article highlights

- A uniaxial stress monitoring method is proposed to catch the field abutment pressure.
- A stress model of coal considering mining and excavation disturbance is proposed.
- The true triaxial stress path in the laboratory to simulate different zones is designed.

🖄 Springer

1 Introduction

The expansion of resource extraction is a national policy for China's scientific and technological innovations. However, the original rock stress balance state is disrupted as coal mining depth increases due to the combined disturbance of roadway excavation and working face mining, and a new equilibrium state is reached by experiencing static or dynamic disturbance stress (Gao et al. 2021; Xie et al. 2021a, b). Hence, mining-induced stresses are a key factor in coal damage. During coal tunnel excavation, excavation unloading affects the stress distribution in the quarry and the mechanical properties of the coal rock. Moreover, the redistribution of stresses can damage the surrounding rock, resulting in micro and macro cracks in the openings and even spalling of the excavated face (Gao et al. 2020; Zheng et al. 2023). In the deep high-ground stress environment, various engineering problems, such as large deformation of soft rock, rock bursts of brittle rock mass, and gas outbursts, may be induced (Feng et al. 2018; Golshani et al. 2009; Kaiser and Moss 2022; Martino and Chandler 2004). The deformation and damage law and the mechanical behavior of coal rock during real complex in situ stress path evolution under a disturbed stress state are considered significant to the mechanical calculation of deep rock mass and the prevention and control of geological disasters in deep mine engineering.

Most underground engineering rocks are in a triaxial stress state. Moreover, underground tunneling and coal mining are typical loading and unloading processes in one or several directions. The stress path of rock experienced has a significant influence on the damage and failure processes of the rock (Bai and Tu 2019; Bai et al. 2022; Wang et al. 2019; Zhang et al. 2018a). For a given conditions, the failure evolution of the rock surrounding the excavation often depends on the stress path. Underground roadway excavation not only creates loading stresses in the rock mass, but also unloading near the excavation boundary (Cong et al. 2020; Zheng et al. 2017). And the loading failure of rocks is not the same as unloading destruction.

Different loading and unloading stress paths have an impact on the mechanical properties of rocks during deformation and failure (Cong et al. 2016). Based on this, scholars have conducted many studies. Field tests (Jayanthu et al. 2004; Kaiser et al. 2001; Wegmuller et al. 2004), numerical simulations (Gao et al. 2015; Rezaei et al. 2015; Yasitli and Unver 2005), and theory models (Alehossein and Poulsen 2010) were developed to explore the influences of mining-induced stress.

Underground coal rocks generally experience disturbances imposed by mining and shaft excavation. Deep coal bears abutment stress σ_v, normal stress of the mining face σ_{n1}, and normal stress of the tunnel surrounding the rock σ_{n2} in three directions. However, the conventional pseudo-triaxial test facility can only apply the abutment and normal stresses of the mining face in two directions (Xie et al. 2012). The true triaxial testing machine has the advantage of applying disturbances in three directions and simulating the real stress conditions of coal in the laboratory. Studies using true triaxial tests on coal samples have mostly concentrated on seepage characteristics and fluid–solid coupling responses (Perera et al. 2013; Ranjith et al. 2011; Shukla et al. 2012). A few studies have tried to explore the mechanical characteristics of underground coal. Alexeev et al. (2004) developed true triaxial loading (TTAL) apparatuses and identified the effects of methane and water absorption on a simulated coal burst. Furthermore, they used TTAL to discuss alterations in the mechanical performances of coals in different stress states, the effect of the stress state on methane emission kinetics from coals at various temperatures, and the effect of moisture content on the mechanical behaviors of coals in different stress states (Alexeev et al. 2012). Connell et al. (2010) studied the permeability analytical model of coal under triaxial strain and stress conditions. Kwasniewski (2013) presented the true triaxial compression test results for coal measure samples containing foliation, anisotropic schist, and medium-coarse sandstone. These tests aimed to show the independent effects of the confining stress and intermediate principal stress on the volumetric deformation mode and the dilatant behavior of rocks. Sha et al. (2018) used true triaxial unloading experiments to study the unloading strength and fracture evolution characteristics of high energy storage rock mass under different stress paths and loading rates. It is

found that the macroscopic failure process of marble under true triaxial unloading is significantly different from that under conventional compression test. The strength and failure mode of high energy storage rock mass are controlled by unloading path and unloading rate. Wang et al. (2022) studied the deformation and seepage characteristics of coal under true triaxial loading and unloading. Li et al. (2018) studied TTAL tests regarding coal's acoustic emission (AE) characteristics. He et al. (2017) used a true triaxial test to obtain the jointed coal mass strength, numerically verified the laboratory results, and proposed a new three-dimensional coal mass strength criterion.

Most of the test paths were straightforward one-way loading and unloading due to the complexity of deep engineering excavation and resource exploitation and the difficulty of simulation. Moreover, a complicated stress path evolution test was conducted for resource utilization under extreme ground stress conditions. The stress conditions of the subsurface zone at various distances from the free face were not adequately considered in most of the research.

To study the real disturbance dynamic characteristics and fracture behavior of deep coal rocks, true triaxial simulation and experimental research were conducted to analyze the mechanical properties and fracture behavior of the coal rock body during the evolution of the in situ stress path, fully considering the tunneling and coal seam excavation process. This provides theoretical and technical guidance for deep rock mechanics analysis and disaster prevention.

2 In situ rock physical response experiment and evolution of coal rock stress path during the mining process

2.1 In situ stress monitoring under real disturbance conditions

Xie et al. (2011, 2012, 2016) analyzed the distribution law of abutment pressure in working faces under three typical mining methods. They further obtained the environmental conditions of mining dynamic stress in the presence of the working face, explored the correlation mechanism between the macroscopic mining process and the rock mechanical loading path, and designed the laboratory test loading path following the mechanical process of deep mining. Figure 1
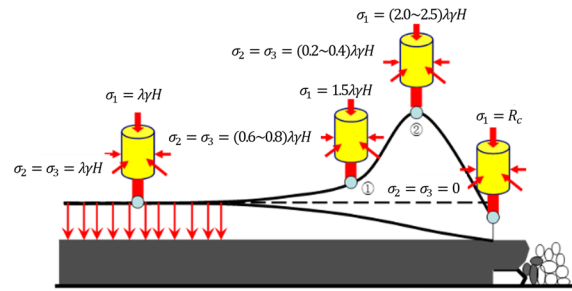

Fig. 1 Stress conditions of coal in front of the working face (Xie et al. 2011)

shows the abutment pressure and normal stress with the mining face changing law of the top coal caving layout. The abutment pressure gradually increases from the hydrostatic pressure to the peak value and then drops to the residual strength with the failure of the coal rock. Moreover, the normal stress σ_{n1} of the mining face decreased from the hydrostatic pressure to 0 MPa. The process can be summarized by formulas 1–3.

$$\text{Original } \sigma_v = \sigma_{n1} = \sigma_{n2} = \gamma H \tag{1}$$

$$\text{Point 1 } \sigma_v = 1.5\gamma H; \; \sigma_{n1} = \sigma_{n2} = (0.6 \sim 0.8)\gamma H \tag{2}$$

$$\text{Point 2 } \sigma_v = (2.0 \sim 2.5)\gamma H; \; \sigma_{n1} = \sigma_{n2} = (0.2 \sim 0.4)\gamma H \tag{3}$$

where σ_v is abutment pressure, σ_{n1} normal stress of mining face, σ_{n2} is normal stress of surrounding rock, γ is vertical stress gradient, H is depth of excavation.

In situ uniaxial stress monitoring was performed at the Tongxin Mine 8309 mining face of the Tong-Mei Group. The test aimed at obtaining the evolution law of field abutment pressure with the advancement of the mining face. We dug a square hole in the free face of the surrounding rock of the roadway and inserted a cylindrical coal sample (50 mm diameter and 100 mm height) from the 8309 working face into the hole. Subsequently, we pushed the sample into the coal using a jack so that the sample was in close contact with the coal rock. With the advancement of the working face, the field abutment pressure applied to the sample was recorded using a GPD450M stress sensor. Figures 2 and 3 show the field arrangement and the installation sample, respectively.
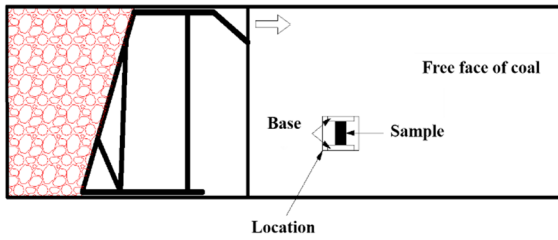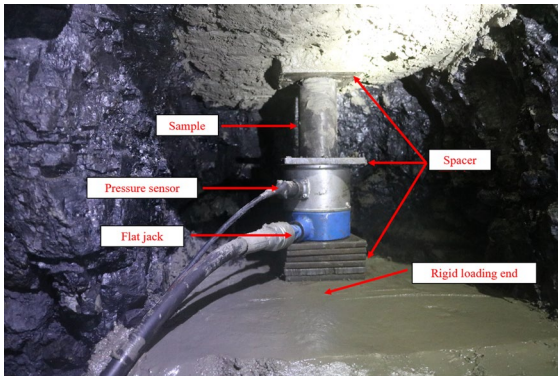
Fig. 2 Stress monitoring test arrangement

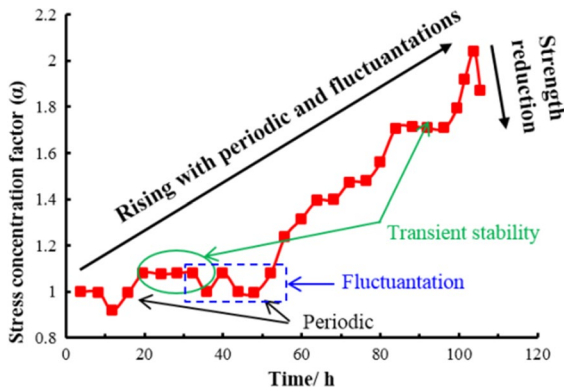**Fig. 3** Installation of the in situ uniaxial sample

Fig. 4 In situ abutment pressure evolution model

We used α to represent the abutment pressure concentration parameter. A change in α reflects the fluctuation and transient stability of the abutment pressure, while the magnitude of α reflects the degree of influence of the mining disturbance. The initial point of α was set to 1 as a benchmark. Consequently, we could calculate α at each time point. Figure 4 shows

the in situ abutment pressure evolution model based on the monitoring results.

With the advancement of the mining face, the periodic increase in abutment pressure reflects stress redistribution. The fluctuation in the abutment pressure curve included downtime for maintenance and personnel handover. Moreover, the cyclic fluctuation in the abutment pressure curve reflected periodic roof weighting. This model considers the working face production status, in situ stress, support conditions, and time effect, reflecting the real condition of the disturbed coal rock. Except for the complicated stress fluctuation, the model based on field monitoring matched the abutment pressure curve in the laboratory (Fig. 1); that is, the stress paths we used in the true triaxial tests corresponded with the real project disturbances. This indicates that our test results were valid and practical.

2.2 Normal stress of surrounding rock and associated zone division criteria

Excavation can change the physical, mechanical and hydraulic properties of the rock zone. Furthermore, it can significantly affect the global rock mass behavior of near fields. The surrounding rocks can be divided into the high excavation-damaged zone (HDZ), excavation-damaged zone (EDZ), and undisturbed zone (UZ) due to different disturbance factors (Fattahi et al. 2013; Kwona et al. 2009; Saiang 2010; Suzuki et al. 2004). Moreover, the stress states of coal rocks in different zones are different. We used the theoretical normal stress from numerical software (FLAC^{3D}) to simplify the stress evolution model and characterize the three zones.

The σ_{n2} stress variation in the surrounding rock was simulated. The width, height, and length of the roadway model were 5 m, 3.6 m, and 50 m, respectively. Furthermore, the entire model's width, height, and length were 25 m, 25 m, and 50 m, respectively. The three-way normal displacement was restricted, 20 MPa pressure relative was applied to the other three faces, and 20 MPa volumetric stress was applied. The tunnel was excavated after the initial equilibration. Moreover, due to the model's symmetry, only a quarter of the model was analyzed. Figure 5a shows the simulation results. After excavation, σ_{n1} gradually increased from 0 MPa to the
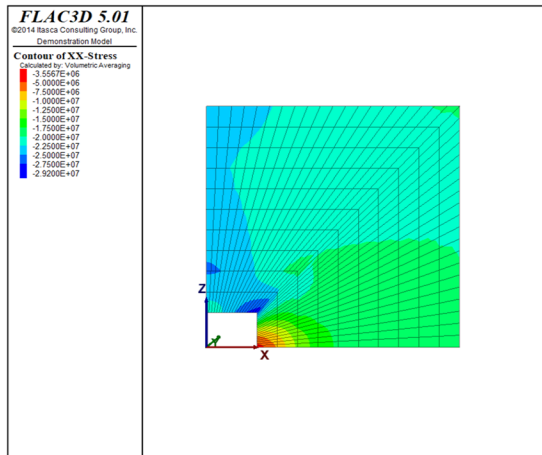
(a) Section of the model (stress contour map of surrounding rock)
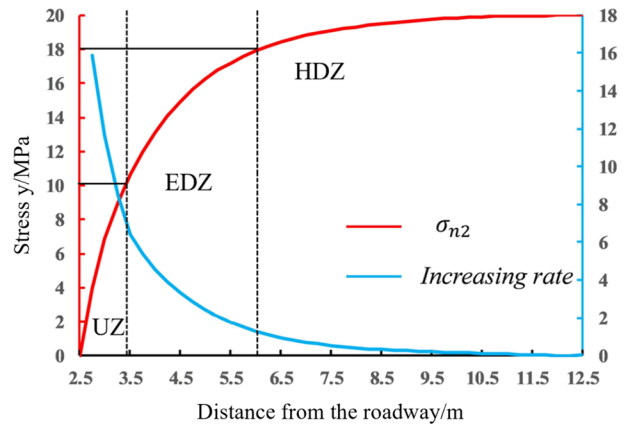
(b) Zone division

Fig. 5 Normal stress results of the numerical model

original rock stress, and the growth rate decreased as the distance from the tunnel increased. Figure 5b shows that the growth rate of σ_{n2} in the surrounding rock tends to slow down when it reaches half of the original rock stress and changes limitedly when it reaches 90% of the original rock stress.

Consequently, based on the original stress, the region where σ_{n2} is 0–50% of the original stress is defined as the HDZ. Furthermore, the region where σ_{n2} is 50–90% of the original stress is defined as the EDZ and the region where σ_{n2} is 90–100% of the original stress is defined as the UZ. Hence, the excavation disturbance effect can be denoted as HDZ > EDZ > UZ.

2.3 Stress model with a top coal caving layout in a disturbed environment

Figure 6 shows that the normal stress σ_{n2} evolution law of the roadway surrounding rock and the abutment pressure σ_v are combined to propose a top coal caving stress model in a disturbed environment. This model can be described as follows: After excavation, the entire stope is divided into the UZ, EDZ, and HDZ, considering the variation in the stress state. Next, the abutment pressure increases to a peak value and then decreases to a residual stress and the normal stress σ_{n1} decreases from the original stress to zero.
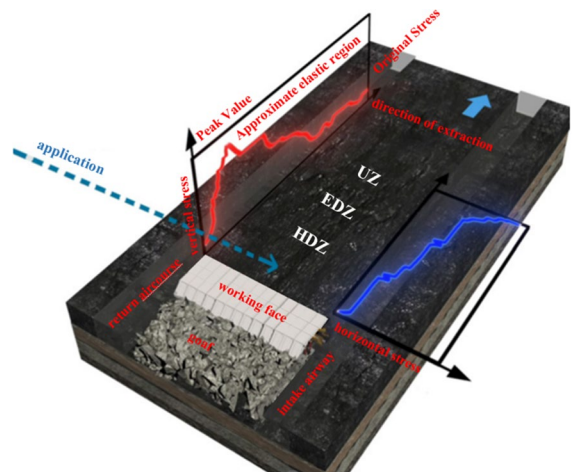

Fig. 6 Stress evolution model under project disturbance

3 True triaxial test and results under a real production disturbance stress path

3.1 Coal cubes and sample preparation

Coal samples were collected from the Tongxin Mine North #3 panel of the TongMei Group at the 8309 mining face at a burial depth of 850 m. The #3–5 coal seams from this mining face are Permo-Carboniferous coal-bearing strata. The coal samples were processed
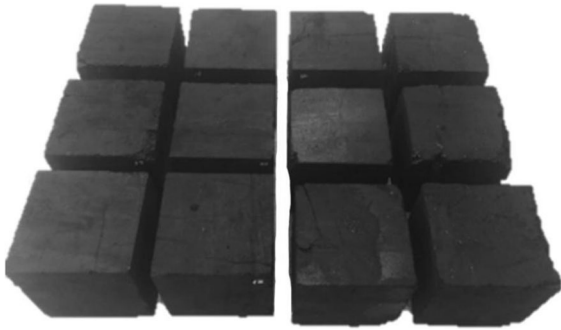
Fig. 7 Cubic samples of coal rock

into cubes with sides measuring 100 ± 0.02 mm (Fig. 7) and then polished to obtain three pairs of mutually parallel faces. We conducted an elemental analysis and identified the basic mechanical properties of the anthracite coal samples; the corresponding results are shown in Table 1 and Table 2, respectively. According to the X-ray diffraction results,

Table 2 Basic mechanical properties of the coal samples

Unconfined test	Density(g/cm^3)	UCS (MPa)	E (GPa)	μ
Average value	1.60	10.12	3.21	0.226

these anthracite coal samples were mainly composed of kaolinite ($Al_2(Si_2O_5)(OH)_4$, 96%) and calcite ($CaCO_3$, 4%).

Experiments were performed on a true triaxial solid–gas coupling experiment system designed by Chongqing University (Fig. 8). Four independent systems were included in the apparatus: a 3D loading stress control system, an internally sealed fluid flow system, an outlet gas flow rate measurement system, and a stress–strain monitoring system. The apparatus can apply 3D stress levels of up to 6000 kN in two directions and 4000 kN in another direction. The 3D deformation of cubic samples was measured within a range of ± 40 mm using six linear variable differential

Table 1 Elemental analysis of the coal samples (unit: percent)

Carbon	Oxygen	Silicon	Aluminum	Sulfur	Iron	Calcium	Potassium
66.71	22.23	4.44	4.37	0.50	0.44	0.14	0.12
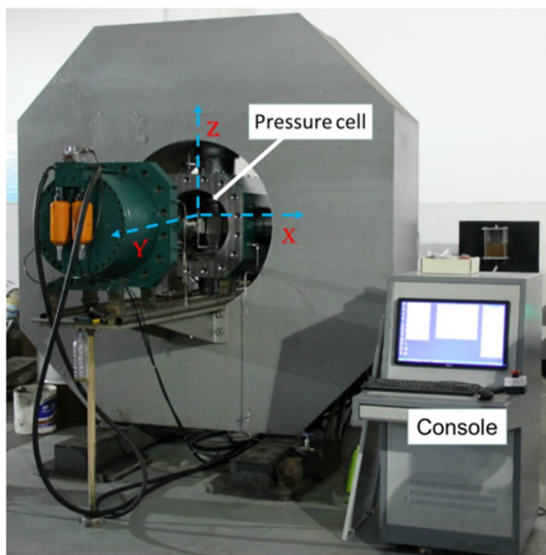
(a) Overall diagram of the system
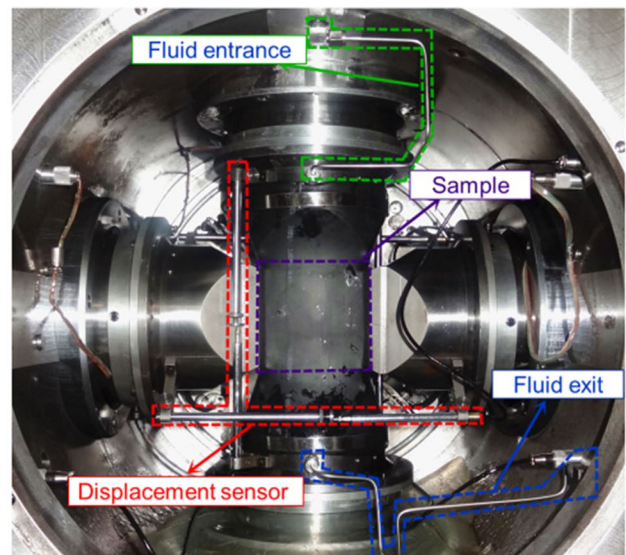
(b) Pressure cell

Fig. 8 True triaxial geophysical apparatus

transformers (LVDTs). The displacement of the loading platens can be measured within a range of ± 8 mm using six LVDT-type displacement transducers. Multiple complete stress paths, including uniaxial, biaxial, and triaxial stress paths, can be applied to study mechanics and seepage (Yin et al. 2016).

3.2 Stress path and experimental procedures

To simulate the mechanical behavior of coal rock in the whole area under the top coal caving using a true triaxial apparatus, abutment pressure σ_v was applied in the direction of σ_1. The normal stress of the mining face σ_{n1} was applied in the direction of σ_2, and the normal stress of the roadway σ_{n2} was applied in the direction of σ_3. Moreover, unloading σ_3 to different ratios to simulate the original stress state before mining different zones and loading σ_1 and unloading σ_2 to simulate increasing abutment pressure and decreasing horizontal stress are integral stress paths.

According to the stress states in different zones and mining unloading effects, experiments were divided into the hydrostatic loading stage, excavation unloading stage, and mining stage to study them separately. The mining stage was divided into two stages according to the two different loading/unloading rates. Table 3 shows the basic information about the samples. The stress path is shown in Fig. 9a–c. The experimental procedures involved the following steps.

The hydrostatic loading stage is denoted as the OA part in Fig. 9. Before the test started, 30 kN of pressure was loaded along the three axes of the sample. Subsequently, a loading rate of 0.2 MPa/s was applied until the loads applied along the three axes were simultaneously 20 MPa. The vertical stress gradient is assumed to be 25 kPa/m. This vertical stress value is equivalent to a depth of approximately 800 m, which

falls within the mining depth of the TongMei Group at the 8309 mining face.

The excavation unloading stage is denoted as the AB part in Fig. 9. Following the normal stress evolution law of the roadway surrounding rock in Part 2.2, this procedure was described separately for the three zones. (I) In the HDZ, σ_3 decreased quickly to $\sigma_3 = 3MPa$, and σ_1 and σ_2 remained unchanged. (II) In the EDZ, σ_3 decreased quickly to $\sigma_3 = 10MPa$, and σ_1 and σ_2 remained unchanged. (III) In the UZ, σ_1, σ_2 and σ_3 remained unchanged for a short time.

In the mining stage, σ_1 increased with a loading rate of 0.1 MPa/s, and σ_2 decreased with an unloading rate of 0.08 MPa/s (Fig. 9a–c, Parts CD and CE). Moreover, σ_1 increased with a loading rate of 0.2 MPa/s, and σ_2 decreased with an unloading rate of 0.08 MPa/s (Fig. 9a–c, Parts DE and EG).

3.3 Mechanical characteristics of coal

The mining dynamic response of the coal rock body at different mining locations was tested to simulate the mining dynamic behavior of the coal rock body at each location. For rock samples in the HDZ and EDZ, σ_1 and σ_2 remained constant while σ_3 was unloaded. Therefore, only the σ_3 unloading part of the stress–strain curves in the excavation unloading stage was selected to compare the unloading effect without considering the mining stage. To compare the effects of mining-induced pressure on three types of rocks, only the mining stage part of the stress–strain curves is selected, and the benchmark of strain is the beginning of the first loading/unloading stage. The benchmark of the strain value in Table 4 is the end of the hydrostatic loading stage.

Figure 10a shows the principal strain–minimum principal stress curve. The unloading rates of T4-18 and T4-5 were the same, but the unloading degrees were different. Therefore, the changing rate of the minimum principal strain is similar, but at the end of this stage, the value of the minimum principal strain of T4-18 is 1.65 times that of T4-5. The increase in the maximum and intermediate strains was caused by the Poisson effect. Figure 10b shows that the strength of the UZ sample is 1.03 times that of the EDZ sample and 1.11 times that of the HDZ sample. Quick unloading of one side of a sample promotes fracture-compacted development, which may have contributed to the weakening

Table 3 Sample details

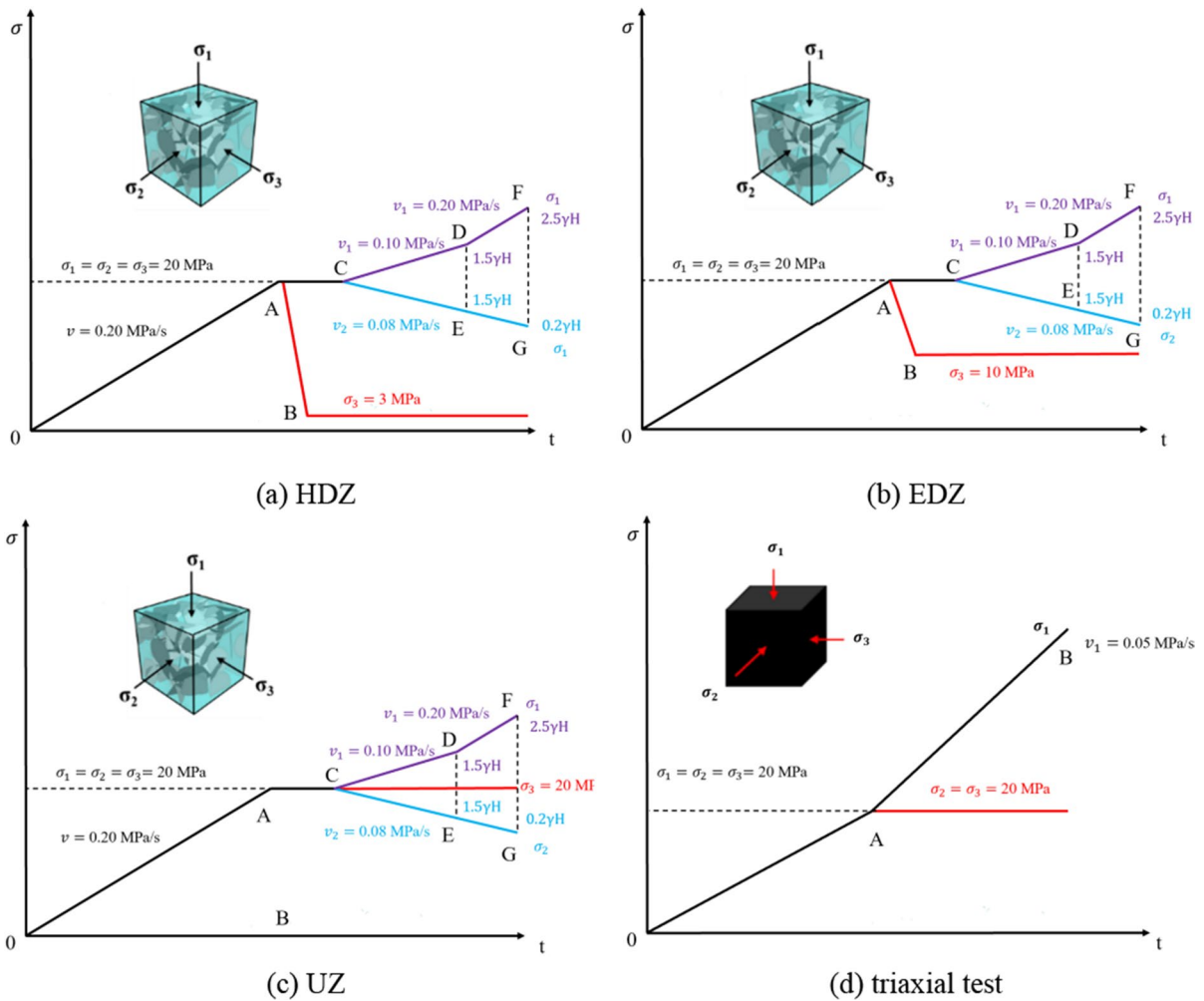| Sample	Location	Density (g/cm^3)	Confining pressure
T3-7	Triaxial test	1.39	20 MPa
T3-28	Triaxial test	1.38	20 MPa
T4-18	HDZ	1.31	20 MPa
T4-5	EDZ	1.31	20 MPa
T4-6	UZ	1.32	20 MPa

Fig. 9 General graph of stress paths in different zones during the mining stage

strength of the samples in the mining stages. This illustrates that a quick unloading of one side's horizontal stress to different degrees could accurately simulate the stress at different distances from the surrounding rock. Therefore, mining simulation can accurately reflect the damage caused by the mining-induced stress of the surrounding rock in different areas.

In the mining stage, according to the stress path shown in Fig. 9, when the maximum principal stress reached 30 MPa, and the intermediate principal stress reached 12 MPa, the first loading/unloading stage finished, and the second loading/unloading stage began. Figure 10b shows that at the end of the first loading/unloading stage, the maximum principal strains of the

samples of the HDZ and EDZ were 1.92 times and 1.89 times that of the UZ sample. At peak stress, the maximum principal strains of the samples of the HDZ and EDZ were 2.30 times and 2.21 times that of the UZ sample. The pressure constraint in the σ_3 direction limited deformation. Thus, to improve the bearing capacity of the surrounding rock and reduce the magnitude of deformation, support measures, such as anchors, should be added to increase the integrity and control deformation through artificially imposed normal stress. The intermediate strains (Fig. 10b) of the three zone's samples are similar, which suggests a weak link between the unloading in the σ_3 direction and the maximum or intermediate principal strain. However, the intermediate principal strain differed
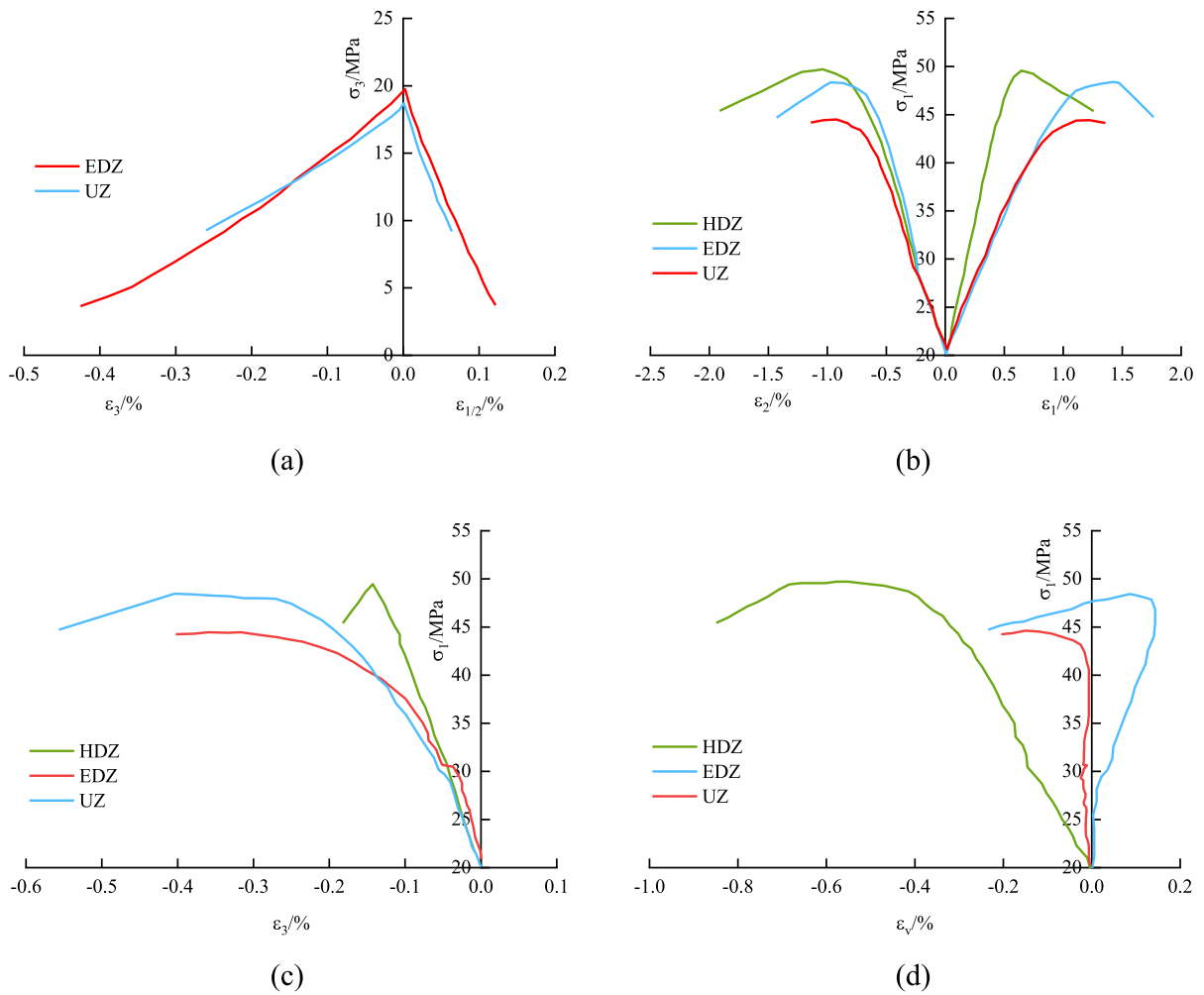
Fig. 10 Stress–strain curves of true triaxial tests: **a** minimum principal stress-principal strain curves for the excavation unloading stage **b** maximum principal stress-maximum and intermediate strain curves for the mining stage **c** maximum principal stress-minimum strain curves for the mining stage **d** the maximum principal stress-volumetric strain curves for the mining stage

in the second loading/unloading stage, 0.91 and 0.88 times that of the UZ sample for the HDZ and EDZ samples, respectively. The UZ sample was unloaded in one direction, and the other two samples were unloaded in two directions, resulting in an enormous intermediate principal strain. The excavation disturbance was responsible for the surrounding rock deformation; thus, it is vital to include roadway excavation disturbance in studying the mechanical characteristics of coal in the mining process.

Meanwhile, Fig. 10d shows that the volumetric strain of the HDZ sample remains constant before the peak stress and expands when the peak stress is reached, the EDZ sample compresses before the peak stress and expands at the peak stress, and the volume of the UZ sample expands throughout the test. Therefore, mining-induced pressure is a risk factor for fracture development for intact rock. The volumetric strain of the UZ sample was much higher than those of the other two. The fracture developed during the excavation unloading stage for the HDZ and EDZ samples, and the fracture development in the mining stage was not obvious in the UZ sample. The peak stress–strain in Table 4 is selected to draw the total trend of principal strain in different regions, as shown in Fig. 11. With the increase of distance from

Table 4 Strain of each stage of the three mining zones (unit: percent)

Sample	Peak stress	Excavation unloading stage				Peak strain				$(\Delta\varepsilon = \varepsilon_{EUS} - \varepsilon_{PV})$			
		ε_1	ε_2	ε_3	ε_v	ε_1	ε_2	ε_3	ε_v	ε_1	ε_2	ε_3	ε_v
T4-18	44.57	0.13	0.12	−0.45	−0.20	1.27	−0.82	−0.78	−0.33	1.14	−0.94	−0.33	−0.13
T4-5	48.38	0.09	0.06	−0.27	−0.12	1.47	−0.85	−0.65	−0.03	1.38	−0.91	−0.38	0.09
T4-6	49.68	–	–	–	–	0.63	−1.04	−0.14	−0.55	0.63	−1.04	−0.14	−0.55

Fig. 11 Comparison of the strength and strain among the three different zones
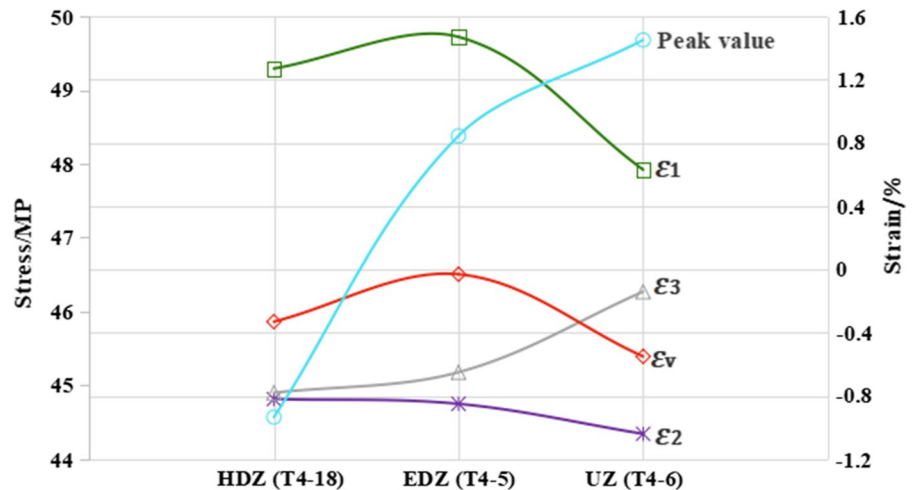
the roadway, the peak stress gradually increases, and the surrounding rock strength is UZ > EDZ > HDZ. It shows that the excavation disturbance has a direct effect on the mechanical behavior of the rock and reduces the strength of the rock.

3.4 Failure morphology and fracture development characteristics of coal rock

Intact coal usually contains preexisting cracks, and the true triaxial loading and unloading process induces the gradual development of the original microcracks until the final failure and the formation of macroscopic cracks. According to the block theory, the structural behavior of discontinuous fractured samples is different from that of intact samples (Liu et al. 2023; Zhang et al. 2021). The six faces of the sample were marked as Sides 1–6, where Sides 1 and 2 are perpendicular and bore the maximum principal stress σ_1; Sides 3–6 were subjected to the confining pressure. The opposite of Side 3 is Side 4, and the opposite of Side 5 is Side 6 (Fig. 12). We extracted surface cracks in coal samples by image processing
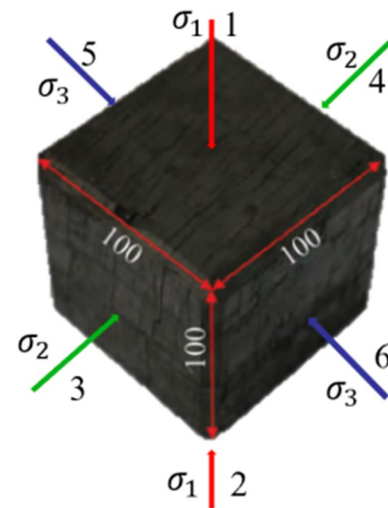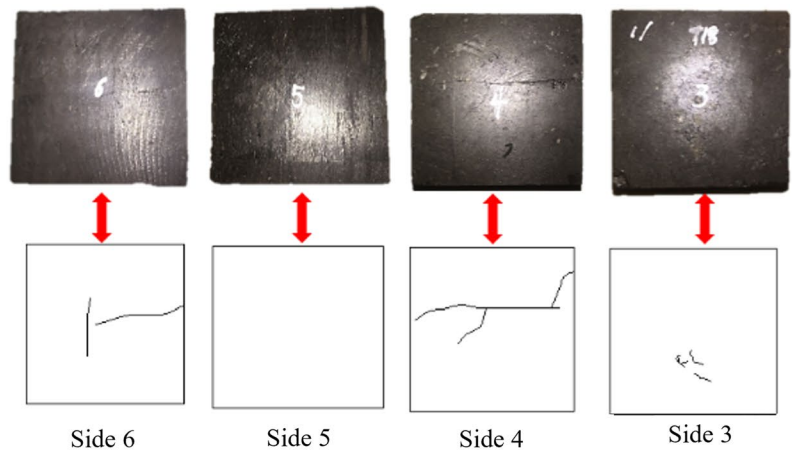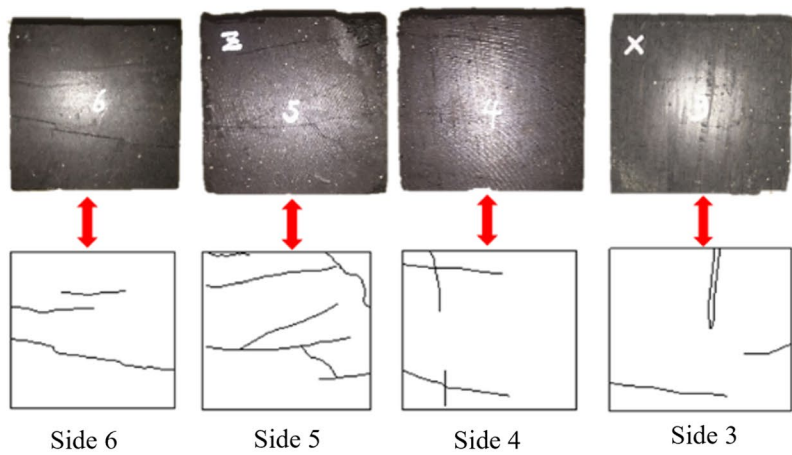

Fig. 12 Sample surface number

and manually copied the original fracture (Fig. 13) and the fracture after the experiments (Fig. 14). The main fractures in the samples are depicted by red dashed lines, and the associated secondary fractures
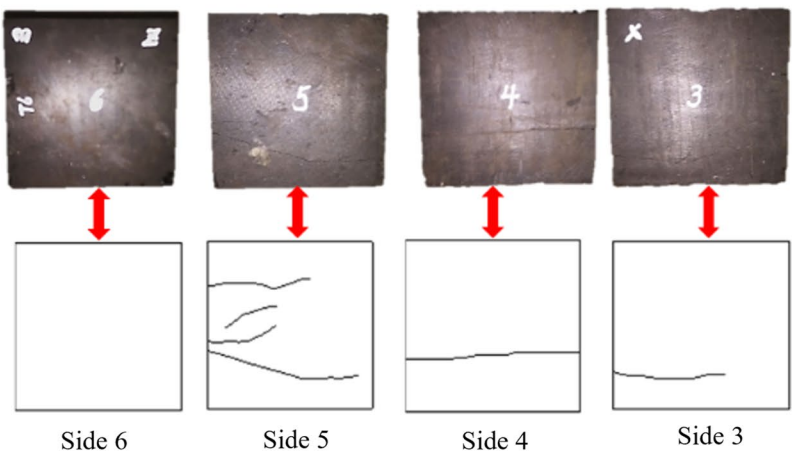
Fig. 13 Original crack distribution of samples before a true triaxial test

Side 6   Side 5   Side 4   Side 3

(a) The HDZ sample

Side 6   Side 5   Side 4   Side 3

(b) The EDZ sample

Side 6   Side 5   Side 4   Side 3

(c) The UZ sample

(a) The HDZ sample

(b) The EDZ sample

(c) The UZ sample
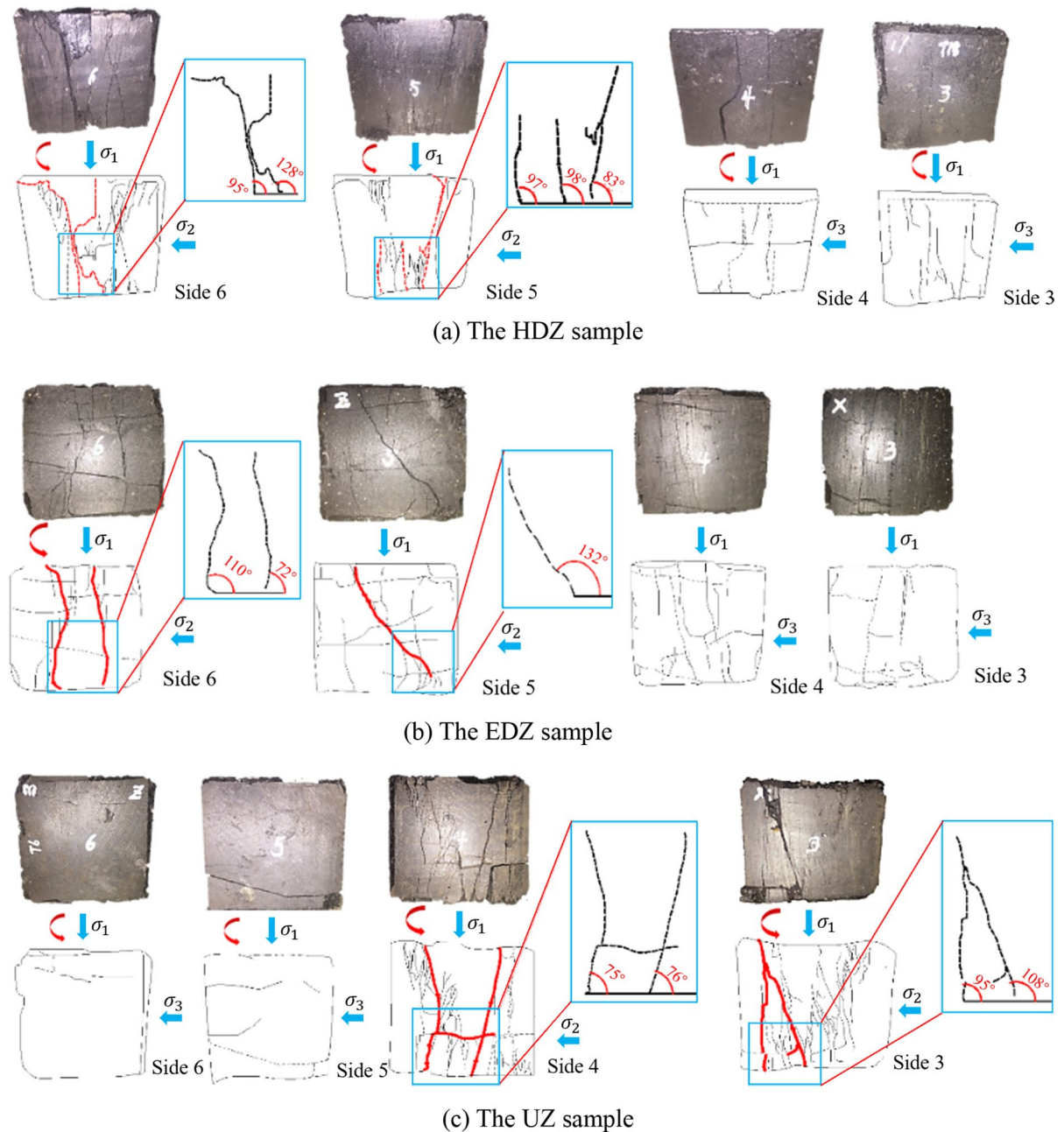
Fig. 14 Crack distribution of samples after a true triaxial test

are depicted by solid lines. One or two shear bands contributed to the failure of each sample. The direction of the shear band with a 70°–130° angle to horizontal was similar to the direction of the maximum principal stress. Under true triaxial loading and unloading condition, the failure surface of the HDZ sample is smooth, without the concave and convex surface caused by the friction between particles. It shows the "I" type tensile splitting failure characteristics, forming a step-like tensile failure surface. The EDZ sample has a rough failure surface, showing a half "X" type failure surface and forming a step-like

single shear failure surface. The UZ sample has a rough failure surface, showing a half "X" type failure surface and forming a single shear failure surface.

Through the fracture morphology and fracture development of the coal sample failure surface, the following rules were determined: (1) With the increase of distance from mining face, the surrounding rock is affected by disturbance, and the failure form of coal sample gradually transitions from tensile failure to shear failure. This is because the HDZ samples are significantly affected by roadway excavation unloading. However, EDZ and UZ samples are far away from the mining face and less affected by mining disturbance. The failure is mainly caused by σ_1 continuous loading and σ_2 continuous unloading. (2) The rock surface that bore the intermediate principal stress in all three zones (Side 4 or 3 of T4-18, Side 4 or 3 of T4-5, Side 6 or 5 of T4-6) had fewer cracks than that of the rock surface that bore minimum principal stress (Side 5 or 6 of T4-18, Side 5 or 6 of T4-5, Side 3 or 4 of T4-6) because the main stage of fracture evolution is the mining stage. (3) The original fracture and stress conditions are important driving factors of rock failure characteristics. The top of Side 4 of T4-18 initially had a horizontal crack, which did not develop into a major crack, while a horizontal crack on the top of Side 4 of T4-6 developed into a major crack due to the difference in the stress path. Side 4 of T4-18 bore σ_2 and experienced

the unloading stage, but that side of the T4-6 bore σ_3 with a stress constraint.

4 Acoustic emission and energy characteristics of rock under true triaxial loading and unloading

Under the action of external force, rock material produces deformation and internal cracks and releases energy simultaneously. Part of its energy is released as a transient elastic wave, thus generating the AE phenomenon. It reflects the degree of damage to rock material and the damage evolution characteristics of rocks (Zhang et al. 2018b, 2021). Therefore, the PCI-2 acoustic emission system was used to monitor the acoustic emission signals in the true triaxial loading and unloading test. Rock AE tests were conducted on the HDZ, EDZ, and UZ samples. Cumulative ringing count and cumulative energy were selected as typical AE characterization parameters to analyze the crack evolution law of coal and rock under true triaxial loading and unloading conditions.

4.1 Analysis of acoustic emission characteristics

The cumulative ringing count can roughly reflect the signal intensity and frequency, which is often used as the AE characteristic parameter to evaluate AE

Fig. 15 AE cumulative ringing count change curve
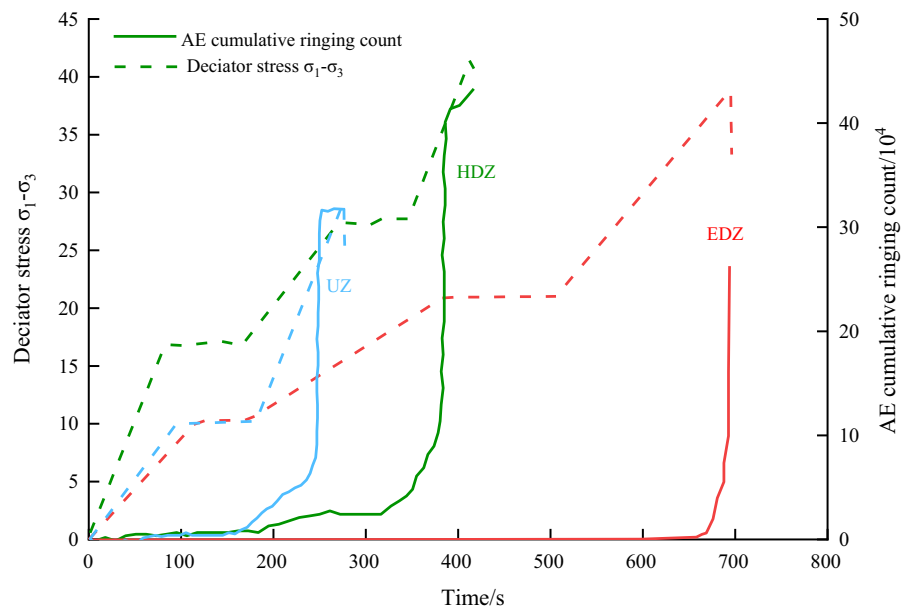
activity, and its value is greatly affected by the AE threshold value. In this monitoring process, the AE monitor threshold was set at 55 dB. Figure 15 shows the change curves of the AE cumulative ringing count of coal samples in different zones under true triaxial loading and unloading. In the unloading stage, as the σ_3 reduces, the deviator stress ($\sigma_1 - \sigma_3$) gradually increase, and AE cumulative ringing counts gradually increase, but with slow growth. In the unloading stage of AE events, when near destruction, numerous microcracks appear and develop, and finally penetrate to form a macroscopic failure surface, and the AE accumulates ringing counts in the process of rapid growth. There is a constant-pressure process for some time between different loading and unloading stages, and the load applied in the three directions of the sample remains unchanged during the constant-pressure process. There is a long period of stabilisation between the different loading and unloading stages, during which the load applied to the sample remains constant in all three directions. The curve of the AE cumulative ringing count during this process is basically parallel to the horizontal axis. It indicates that the AE cumulative ringing count of the sample remains constant during the steady pressure process, and the coal sample is in a relatively stable mechanical state. The cumulative ringing count when the HDZ sample is damaged is 43.06×10^4 times. When

the EDZ sample is damaged, the cumulative ringing count is 26.37×10^4 times. Furthermore, the cumulative ringing count when the UZ sample is damaged is 31.87×10^4 times.

The test results show that the cumulative AE ringing count is the highest when the HDZ sample is damaged. This indicates that the AE events are the most during the failure of HDZ sample, and there are more microcracks in the sample. However, the cumulative AE ringing count of HDZ, EDZ and UZ samples does not show obvious regularity when the three samples were destroyed. This may be due to the fact that coal rock itself is a heterogeneous material. In the process of coal formation, the internal structure is different from the occurrence of primary cracks. As a result, the new crack generation and primary crack development of different samples are affected to different degrees during loading and unloading.

4.2 Energy characteristics under true triaxial loading and unloading

The AE cumulative energy can reflect the relative energy and intensity of events, indirectly reflect the magnitude of AE events, and measure the internal damage and fracture degree of rock samples during the test. Figure 16 shows the change

Fig. 16 AE cumulative energy change curve
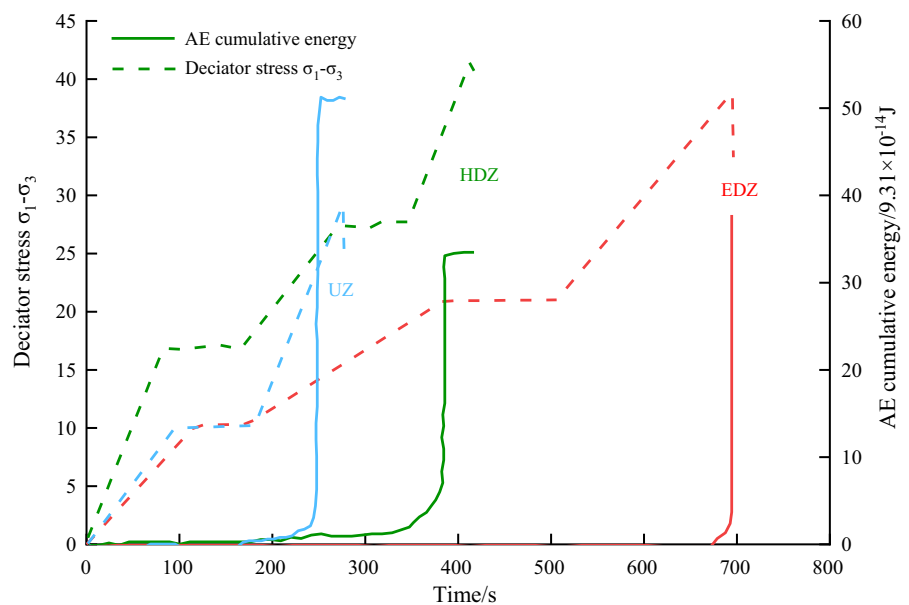
curves of the AE cumulative energy of coal samples in different zones under true triaxial loading and unloading. In the unloading stage σ_3 and the first unloading stage of roadway excavation, the deviatoric stress $(\sigma_1 - \sigma_3)$ increases with the decrease of σ_3, and the accumulated AE energy of different coal samples increases slowly. In the second unloading stage, when the failure is near, the AE events greatly increase, and numerous microcracks are generated, developed, and finally connected to form a macroscopic failure surface. During this process, cumulative energy increases sharply within a short time. The cumulative energy when the HDZ coal sample is damaged is 3.11×10^{-12} J, the cumulative AE energy when the EDZ coal sample is damaged is 3.51×10^{-12} J, and the cumulative energy when the UZ sample is damaged is 4.75×10^{-12} J.

The AE test results show that UZ sample releases the most energy in a short time while the cumulative ringing count is less. It indicates that the UZ sample produces more AE events with large energy during failure, resulting in more obvious macro cracks, and fewer internal micro cracks. The macro failure form of coal sample is more complex, and the degree of failure is more intense. The cumulative AE energy of HDZ sample was lower, but the cumulative ringing count was higher. This indicates that there are more AE events with small energy during the failure of HDZ sample and more microcracks during the failure of the sample. Similarly, the AE cumulative energy of three samples, HDZ, EDZ and UZ, does not show obvious regularity during failure. In the future, tests can be carried out under different surrounding rock and different loading and unloading rates.

There is a certain correlation between macroscopic failure pattern and microcrack evolution characteristics of coal rock. The formation and development of cracks on the surface and inside of coal rock is the fundamental cause of macroscopic deformation and failure. When the coal sample is damaged, the higher the AE cumulative ringing count or AE cumulative energy is, the more cracks are developed inside the coal rock, and the macro failure form is more complex. Therefore, microseismic monitoring can be carried out in the field

to predict the possible rock burst, large caving and other macro damage in the production process.

5 Comparative analysis of triaxial and true triaxial research results

5.1 Mechanical characteristics of conventional triaxial samples

Following the stress path evolution of in situ rock during mining, we obtained true triaxial experimental results regarding the influence of mining disturbance. Furthermore, we conducted a conventional triaxial experiment in the laboratory according to the stress path of coal and rock to obtain the failure results of coal samples without considering the influence of mining disturbance; this was to obtain a more accurate comparison of the influence of mining disturbance stress on the failure of coal samples. The apparatuses used for these tests were the same as those used for the tests above. Figure 9d shows the tested stress path, and the sample details are listed in Table 3.

Figures 17 and 18 and Table 5 show the resulting stress–strain curves, failure modes, and parameters. The two samples exhibited relatively consistent mechanical behavior.
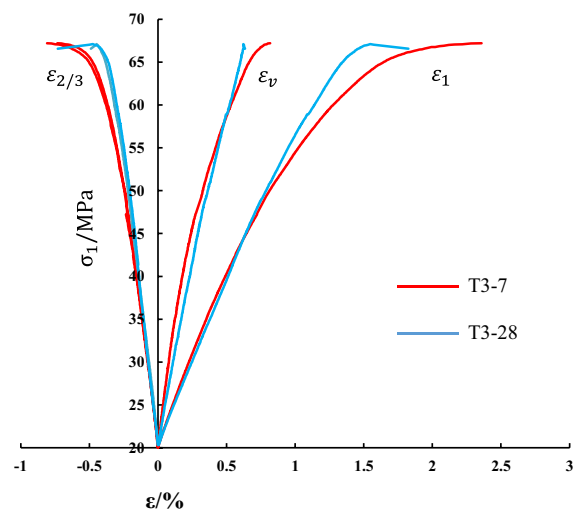

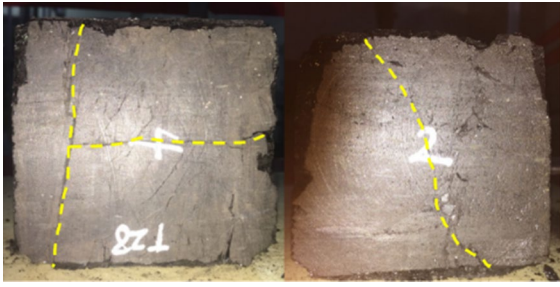**Fig. 17** Stress–strain curves from the cubic triaxial tests

Fig. 18 Destroyed cubic triaxial test sample (T3-28)

5.2 Comparative analysis of the mechanical behavior and damage characteristics of coal rocks under conventional triaxial and true triaxial mechanics

1. Mechanical parameters

Comparing the triaxial tests with the true triaxial tests, it can be observed that the average strength of the cubic triaxial test samples increased by more than 36% compared to that of the UZ sample (T4-6). The maximum principal strain increased 2.75 times compared to that of Sample T4-6. The volume of the cubic samples consistently decreased, while that of Sample T4-6 decreased first and then expanded. Furthermore, the deformation in the cubic samples is much smaller than in true triaxial tests, considering the mining loading/unloading process. Shallow cracks were observed on the surface of the samples, and the rocks did not split into pieces. Shear failure was observed in the cubic triaxial test.

2. Macroscopic failure type

Under conventional triaxial compression conditions, the macroscopic failure modes of coal samples were mainly half "X" and half "Y," that is, pure shear failure or tensile shear composite failure. The number of microcracks on the surface of the coal sample was small after destruction, and the coal sample remained relatively intact. In addition, since the stress concentration around the corner of the cubic coal sample, coal flakes, and small coal samples fell off at this position, the macrocracks of coal sample failure began to extend and develop from the drop position spreading through the whole sample.

During the true triaxial test, the HDZ coal sample was subject to overall instability in the second unloading stage. It showed obvious "I" type failure characteristics and belonged to tensile splitting failure. The main failure surface was perpendicular to σ_3 unloading direction. The EDZ sample was subject to overall instability in the second unloading stage. Although the coal and rock masses at this location were affected by the tunnel excavation σ_3 was reduced by half, but the failure of coal samples under low confining pressure was mainly due to σ_1 continuous loading and σ_2 caused by continuous unloading. The coal sample mainly presented half "X" type failures, belonging to pure shear failure or tension shear composite failure. For the UZ sample, during the whole test σ_3 remained the same; the failure of coal samples was mainly caused by σ_1 continuous loading and σ_2 caused by continuous unloading. The coal sample mainly presented half "X" type failures, belonging to pure shear failure or tension shear composite failure.

3. Deformation features

During the triaxial test, the coal samples showed significant linear elastic deformation characteristics in the initial state. The strain of the horizontal direction of the coal sample (σ_2 and σ_3) remained the same throughout the deformation failure process, and the overall volume compression was always maintained

Table 5 Cubic triaxial test parameters

Sample	Peak				Difference with T4-6		
	Peak stress	Maximum principal strain	Minimum principal strain	Volumetric strain	Peak stress	Maximum principal strain	Volumetric strain
T3-7	67.19	2.36	−0.73	0.82	+17.51	+1.73	+1.37
T3-28	67.10	1.55	−0.45	0.62	+17.42	+0.92	+1.17
Average	67.15	1.96	−0.59	0.72	+17.47	+1.33	+1.27

relative to the initial state. However, during the true triaxial test, after the EDH sample entered the first unloading stage, it was affected by the superposition of σ_1 loading and σ_2 unloading, the compression deformation in the σ_1 direction continued to increase. Furthermore, the strain in the direction of σ_2 showed an inflection point and began to change from compression deformation to expansion deformation.

Consequently, the cubic triaxial test with a stress path of $\sigma_1 > \sigma_2 = \sigma_3$ cannot simulate real disturbing stress conditions in coal mining.

5.3 Comparison of the triaxial tests and the true triaxial tests with mining loading/unloading stages

Xie et al. (2012) explored the mechanical characteristics of rock during mining with a top coal caving layout. Their tests used the MTS 815 Flex Test GT rock mechanical system, and samples were from the 8105 mining face of the Tashan Mine of Datong Mining Group. The procedure of the tests was as follows: Loading is first applied to create a confining pressure of 25 MPa; subsequently, the same stress path as that used in the mining stage of the true triaxial tests is used. The results are shown in Fig. 19. Unlike the continuous expansion of Sample T4-6, the volumetric strain gained from the triaxial machine causes the sample to compress and then expand. A large difference in the intermediate

Fig. 20 Relationship between b and the stress ratio of the initial expansion point

parameter $b = (\sigma_2 - \sigma_3)/(\sigma_1 - \sigma_3)$ between these two tests resulted in differences in the trend of the volumetric strain.

At peak stress, the intermediate parameter b of the samples correlating to the three zones increased with increasing integrity (Fig. 20), but the σ_{iep}/σ_p ratio did not show an obvious changing law. Meanwhile, the ratio of the loading and unloading rates is the key factor controlling the failure mode. When the stress path was the same as that of Sample T4-6 but with a minimal loading and unloading rate ratio, the sample volume was continuously compressed (Liu et al. 2019).

True triaxial test is different from conventional triaxial test. The fracture mechanism of coal rock under true triaxial loading and unloading considering disturbance factors is still a direction to be further studied. In the future, true triaxial tests of coal rock in different regions at different loading and unloading rates and under different surrounding rock conditions can be carried out to further study the fracture mechanism of coal rock under the influence of mining disturbance, and the true triaxial strength criterion applicable to the excavation disturbance conditions of coal rock can be proposed.

6 Conclusion

Roadway excavation and mining processes influence the mechanical characteristics of coal rock. In this research, a stress evolution model of underground coal and the stress path to realizing the model in the laboratory were proposed, and the following conclusion was reached:

Fig. 19 Triaxial test curves considering the mining stages of a top coal caving layout (from (Xie et al. 2012))

1. The true triaxial stress–strain curves of the three zones showed that the strengths of three samples are UZ > EDZ > HDZ. The expansion in the unloading direction in the HDZ sample was larger than that of the EDZ sample, which illustrates that the methods of unloading to different degrees could represent the original stress condition and bearing capacity of the coal in the whole stope before the mining process.

2. The mining stage curves showed that the maximum principal strains of the HDZ and EDZ samples were 2.30 and 2.21 times that of the UZ sample at peak stress, respectively. The volume of the UZ sample continued to expand throughout the test. Furthermore, the volume of the HDZ and EDZ samples expanded after peak stress was reached. The shear bands ultimately caused the failure of these samples.

3. The strength of cubic triaxial test is obviously higher than that of true triaxial tests, but the destruction is smaller than that of true triaxial test. In contrast with the continuously expanding volume of the samples of the true triaxial test, the volume of samples during pseudo triaxial tests under the stress path of the top coal caving layout decreased and then increased. The surfaces in the σ_{n2} direction of the samples have considerably more cracks than the other surfaces for all three zones.

Declarations

References

Alehossein H, Poulsen BA (2010) Stress analysis of longwall top coal caving. Int J Rock Mech Min Sci 47:30–41

Alexeev AD, Revva VN, Alyshev NA, Zhitlyonok DM (2004) True triaxial loading apparatus and its application to coal outburst prediction. Int J Coal Geol 58:245–250

Alexeev AD, Revva VN, Molodetski AV (2012) Stress state effect on the mechanical behavior of coals under true triaxial compression conditions. International Workshop on the True Triaxial Testing of Rocks, Beijing, pp 281–291

Bai Q, Tu S (2019) A general review on longwall mining-induced fractures in near-face regions. Geofluids 2019:3089292

Bai Q, Zhang C, Young RP (2022) Using true-triaxial stress path to simulate excavation-induced rock damage: a case

study. Int J Coal Sci Technol 9:49. https://doi.org/10.1007/s40789-022-00522-z

Cong Y, Feng X, Zheng Y, Wang Z, Zhang L (2016) Experimental study on acoustic emission failure precursors of marble under different stress paths. Chin J Geotech Eng 37:1193–1201

Cong Y, Wang Z, Zheng Y, Zhang L (2020) Effect of unloading stress levels on macro-and microfracture mechanisms in brittle rocks. Int J Geomech 20:04020066

Connell L, Lu M, Pan Z (2010) An analytical coal permeability model for tri-axial strain and stress conditions. Int J Coal Geol 84:103–114

Fattahi H, Shojaee S, Mohammad AEF, Mansouri H (2013) Hybrid Monte Carlo simulation and ANFIS-subtractive clustering method for reliability analysis of the excavation damaged zone in underground spaces. Comput Geotech 54:210–221

Feng XT, Guo HS, Yang CX, Li SJ (2018) In situ observation and evaluation of zonal disintegration affected by existing fractures in deep hard rock tunneling. Eng Geol 242:1–11. https://doi.org/10.1016/j.enggeo.2018.05.019

Gao F, Stead D, Kang H (2015) Numerical simulation of squeezing failure in a coal mine roadway due to mining-induced stresses. Rock Mech Rock Eng 48:1635–1645

Gao MZ, Wang MY, Xie J, Gao YN, Deng GD, Yang BG et al (2020) In-situ disturbed mechanical behavior of deep coal rock. Journal of the China Coal Society 45:2691–2703

Gao MZ, Chen L, Fan D, Yang MQ, Liu C, Li JN et al (2021) Principle and technology of coring with in-situ pressure and gas maintaining in deep coal mine. J China Coal Soc 46:885–897

Golshani A, Oda M, Okui Y, Takemura T, Munkhtogoo E (2009) Numerical simulation of the excavation damaged zone around an opening in brittle rock. Int J Rock Mech Min Sci 44:835–845

He PF, Kulatilake PHSW, F.ASCE;, Liu DQ, He MC. Development of new three-dimensional coal mass strength criterion. Int J Geomech. 2017;17.

Jayanthu S, Singh TN, Singh DP (2004) Stress distribution during extraction of pillars in a thick coal seam. Rock Mech Rock Eng 37:171–192

Kaiser PK, Yazici S, Maloney S (2001) Mining-induced stress change and consequences of stress path on excavation stability—a case study. Int J Rock Mech Min Sci 38:167–180

Kaiser PK, Moss A (2022) Deformation-based support design for highly stressed ground with a focus on rockburst damage mitigation. J Rock Mech Geotech Eng 14:50–66. https://doi.org/10.1016/j.jrmge.2021.05.007

Kwasniewski M (2013) Recent advances in studies of the strength of rocks under true triaxial compression conditions. Arch Min Sci 58:1177–1200. https://doi.org/10.2478/amsc-2013-0080

Kwona S, Leeb CS, Choc SJ, Jeonb SW, Choa WJ (2009) An investigation of the excavation damaged zone at the KAERI underground research tunnel. Tunn Undergr Space Technol 24:1–13

Li DX, Wang EY, Kong XG, Wang XR, Zhang C, Jia HH et al (2018) Fractal characteristics of acoustic emissions from coal under multi-stage true-triaxial compression. J Geophys Eng 15:2021–2032

Liu YB, Yin GZ, Li MH, Zhang DM, Deng BZ, Liu C et al (2019) Anisotropic mechanical properties and the permeability evolution of cubic coal under true triaxial stress paths. Rock Mech Rock Eng 52:2505–2521

Liu YB, Wang EY, Jiang CB, Zhang DM, Li MH, Yu BC et al (2023) True triaxial experimental study of anisotropic mechanical behavior and permeability evolution of initially fractured coal. Nat Resour Res. https://doi.org/10.1007/s11053-022-10150-8

Martino JB, Chandler NA (2004) Excavation-induced damage studies at the Underground Research Laboratory. Int J Rock Mech Min Sci 41:1413–1426

Perera M, Ranjith P, Choi S (2013) Coal cleat permeability forgas movement under triaxial, non-zero lateral strain condition: atheoretical and experimental study. Fuel 109:389–399

Ranjith P, Perera M (2011) A new triaxial apparatus to study the mechanical and fluid flow aspects of carbon dioxide sequestration in geological formations. Fuel 90:2751–2759

Rezaei M, Hossaini MF, Majdi A (2015) Determination of longwall mining-induced stress using the strain energy method. Rock Mech Rock Eng 48:2421–2433

Saiang D (2010) Stability analysis of the blast-induced damage zone by continuum and coupled continuum–discontinuum methods. Eng Geol 116:1–11

Sha P, Wu FQ, Chang JY (2018) Unloading strength and failure pattern of marble under true triaxial test. Chin J Rock Mech Eng 37:2084–2092

Shukla R, Ranjith PG, Choi SK, Haque A. A novel testing apparatus for hydromechanical investigation of rocks: geosequestration of carbon dioxide. Rock Mech Rock Eng. 2012;45.

Suzuki K, Nakata E, Minami M, Hibino E, Tani T, Sakakibara J et al (2004) Estimation of the zone of excavation disturbance around tunnels, using resistivity and acoustic tomography. Explor Geophys 35:62

Wang C, Zhang D, Yu B, Li S (2022) Deformation and seepage characteristics of coal under true triaxial loading–unloading. Rock Mech Rock Eng. https://doi.org/10.1007/s00603-022-03207-w

Wang SF, Li XB, Yao JR, Gong FQ, Li X, Du K et al (2019) Experimental investigation of rock breakage by a conical pick and its application to non-explosive mechanized mining in deep hard rock. Int J Rock Mech Min Sci 122:104063

Wegmuller U, Werner C, Strozzi T, Wiesmann A. Monitoring mining induced surface deformation. In: 2004 IEEE international geoscience and remote sensing symposium; Anchorage, AK: IEEE; 2004.

Xie HP, Zhou HW, Liu JF, Gao F, Zhang R, Xue DJ et al (2011) Mining-induced mechanical behavior in coal seams under different mining layouts. J China Coal Soc 36:1067–1074

Xie HP, Zhao XP, Liu JF, Zhang R, Xue DJ (2012) Influence of different mining layouts on the mechanical properties of coal. Int J Min Sci Technol 22:749–755

Xie HP, Zhang ZT, Gao F, Zhang R, Gao MZ, Liu JF (2016) Stress-fracture-seepage field behavior of coal under different mining layouts. J China Coal Soc 41:2405–2417

Xie HP, Gao MZ, Fu CH, Lu YQ, Yang MQ (2021a) Mechanical behavior of brittle-ductile transition in rocks at different depths. J China Coal Soc 46:701–715

Xie J, Gao MZ, Zhang S (2021b) Experimental study on triaxial fracture behavior and energy release law of deep coal under the effect of loading rates. J Central South Univ (sci Technol) 52:2713–2724

Yasitli NE, Unver B (2005) 3D numerical modeling of longwall mining with top-coal caving. Int J Rock Mech Min Sci 42:219–235

Yin GZ, Jiang CB, Wang JG, Xu J, Zhang DM, Huang G (2016) A new experimental apparatus for coal and gas outburst simulation. Rock Mech Rock Eng 49:2005–2013

Zhang D, Ai C, Li Y, Che M, Gao R, Zeng J. Energy-based brittleness index and acoustic emission characteristics of anisotropic coal under triaxial stress condition. Rock Mech Rock Eng. 2018b;3343–60.

Zhang R, Liu J, Sa Z, Wang Z, Lu S, Lv Z (2021) Fractal characteristics of acoustic emission of gas-bearing coal subjected to true triaxial loading. Measurement 169:108349

Zhang YT, Ding XL, Huang SL, Qin Y, Li P, Li YJ (2018b) Field measurement and numerical simulation of excavation damaged zone in a 2000 m-deep cavern. Geomech Eng 16:399–413

Zheng G, Du Y, Cheng X (2017) Characteristics and prediction methods for tunnel deformations induced by excavations. Geomech Eng 12:361–397

Zheng Z, Tang H, Zhang Q, Pan PZ, Zhang X, Mei GX et al (2023) True triaxial test and PFC3D-GBM simulation study on mechanical properties and fracture evolution mechanisms of rock under high stresses. Comput Geotech 154:105136

Publisher's Note   Springer Nature remains neutral with regard to jurisdictional claims in published maps and institutional affiliations.